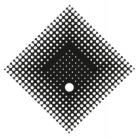
VICTORIA UNIVERSITY
MELBOURNE AUSTRALIA

Optimal sampling requirements for robust and fast vegetation high impedance fault detection

This is the Published version of the following publication

Ozansoy, Cagil and Zayegh, Aladin (2023) Optimal sampling requirements for robust and fast vegetation high impedance fault detection. IEEE Access, 11. pp. 42924-42936. ISSN 2169-3536

The publisher's official version can be found at
https://ieeexplore.ieee.org/document/10109717
Note that access to this version may require subscription.

Downloaded from VU Research Repository https://vuir.vu.edu.au/46877/

IEEE Access
Multidisciplinary | Rapid Review | Open Access Journal

Received 11 April 2023, accepted 20 April 2023, date of publication 27 April 2023, date of current version 5 May 2023.

Digital Object Identifier 10.1109/ACCESS.2023.3270928

RESEARCH ARTICLE

Optimal Sampling Requirements for Robust and Fast Vegetation High Impedance Fault Detection

CAGIL RAMADAN OZANSOY, (Member, IEEE), AND ALADIN ZAYEGH, (Life Member, IEEE)
College of Sports, Health, and Engineering, Victoria University, Melbourne, VIC 8001, Australia
Corresponding author: Cagil Ramadan Ozansoy (cagil.ozansoy@vu.edu.au)

ABSTRACT Low fault currents, associated with Vegetation High Impedance Fault (VeHIF) events, are often challenging to clear by relying on traditional overcurrent based protection schemes. Low Frequency (LF) harmonics have readily been used in the literature as potential fault detection features. High Frequency (HF) signatures are also generated during VeHIFs events. These have generally been underrepresented, potentially for reducing the computational burden and the cost of proposed solutions. This work presents the temporal magnitude growth comparison of the LF and HF fault current spectrums using a dataset of 125 phase-to-earth (ph-to-e) tests. The key focus is on comparing the protection-speed efficacy of the LF and HF fault signatures. For the analysed dataset, the temporal growth in the HF spectral components was determined to be faster in a larger number of tests and with higher average lead-time margins. Conversely, growth in the LF spectral components was faster in fewer tests and with a smaller average lead-time margin. The HF spectrum was the lead indicator in 68.2 % of the 125 ph-to-e test recordings with an average lead-time of 26.95 s. For the same dataset, the LF spectrum was the leading indicator in only 25.6 % of the tests with an average lead-time of 7.85 s. Analysis has also revealed that a sampling frequency, as large as 1.8 MHz, may be required when designing protection applications, where the speed of protection is as critical as robustness.

INDEX TERMS Current signals, high frequency sampling, high frequency signatures, high impedance faults, vegetation faults, speed of detection, statistical analysis.

I. INTRODUCTION

VeHIF events exhibit low fault currents that are often not successfully cleared by overcurrent protection devices in common use in the power utility sector. If undetected, HIFs pose a severe risk to public safety and can ignite fires. The HIF current is branded for its low magnitude, unstable, and fluctuating behaviour with high asymmetry. The use of pattern recognition techniques for the detection of HIF signatures has gained further momentum post the digitisation of protection devices. It is also well known that the detection of earth faults must occur fast to minimise bush-fire risks. This yields a challenge itself in ensuring high security of the employed scheme for minimising false positives. There is always the need to balance security and speed.

The key focus in this work is on the analysis of LF and HF signatures of VeHIFs, specifically in terms of their temporal growth during a VeHIF. This will be undertaken using a large dataset of staged VeHIF tests. "Could the LF or HF signatures enable a faster response to VeHIFs?" is the key research question targeted herein. The work assesses the temporal growth in the LF (DC to 50 kHz) and HF (10 kHz to 1 MHz) spectrums using well-known techniques. These include the Fast Fourier Transform (FFT) and cumulative sum of the magnitudes of a set of frequency components in the two sets of spectra. While acknowledging that standard methods have been used herein, the application of these techniques for the temporal growth comparison of LF and HF current signatures is a novelty and has not been attempted or covered elsewhere. This manuscript does not propose a protection scheme, but seeks to contribute to the body of knowledge in the VeHIF electrical phenomena, particularly in regards to its LF and HF signatures. The intent is to inform industry and academic researchers on the need to consider under-utilised HF signatures for a fast response. Authors acknowledge robustness in the LF components (larger magnitudes), and recommend

The associate editor coordinating the review of this manuscript and approving it for publication was Padmanabh Thakur.

This work is licensed under a Creative Commons Attribution 4.0 License. For more information, see https://creativecommons.org/licenses/by/4.0/

HF and LF components to be considered together to combine speed and robustness.

Researchers have proposed a series of solutions for HIF detection using artificial intelligence [1], multiresolution [2] or statistical methods [3], [4]. LF signature components such as low-order harmonics [5] and their combinations have popularly been used as features to detect such faults using various techniques [1], [6], [7]. VeHIFs often produce High Frequency (HF) signatures that have generally been under-represented in the literature. The idea that the sampling rate needs to be kept low, for reducing the computational burden and the cost, is often a rationale behind the overwhelming focus in LF signal components [8].

The 1982 studies by Aucoin and Russell [9], [10] were the pioneering works that introduced the concept of identifying HF (only 2-10 kHz then) changes associated with arcing HIF currents. The authors argued that arcing HIFs exhibit an increase in the HF components of current over un-faulted systems, which can be used as fault signatures in a detection technique [9], [10]. More recently, Jia et al. proposed a distance protection method based on using the HF fault transients. Their solution relies on extracting HF components of the voltage and current signals to identify the fault and map the faulted section [11]. In this simulation verified study [11], a sampling frequency of 10 kHz was used and the 1–1.6 kHz frequency range was selected as the frequency band. In [12], the authors investigated traveling wave based HF signatures for fault detection and localization in distribution systems. Simulation based validations were presented in [12], where the IEEE 13-bus test system was used for fault analysis. The signals were sampled at 10 MHz for recording the HF signatures using high-pass filtering with a cut-off frequency of 10 kHz. One key conclusion of the study was that HF waves can potentially be used for detecting and locating faults under high Distributed Energy Resource (DER) penetration levels [12]. Jafarian and Sanaye-Pasand presented a protection technique in [13] based on fault generated HF transients. The authors used the wavelet transform and Support Vector Machine (SVM) techniques for fault classification. The current signals were sampled at a sampling frequency of 160 kHz. The measured signals were decomposed into five different frequency bands (40–80 kHz, 20–40 kHz, 10–20 kHz, 5–10 kHz and 2.5–5 kHz) using Discrete Wavelet Transform (DWT) [13].

The work by Gomes et al. proposed a fault detection method based on vegetation fault signatures' HF content. Validation was performed using a real dataset comprising a large number of experiments, sampled in a functioning network in the presence of noise. One key feature of the work separating it from comparable works in the literature was the large bandwidth utilized, from 10 kHz to 1 MHz. This is as compared to other works where narrow bandwidths (few thousand of Hz) of the electric signals' frequency spectrum was used [14]. In a more recent study, the authors presented the application of the shift-invariant sparse coding technique as an effective technique to describe the fault signatures [15].

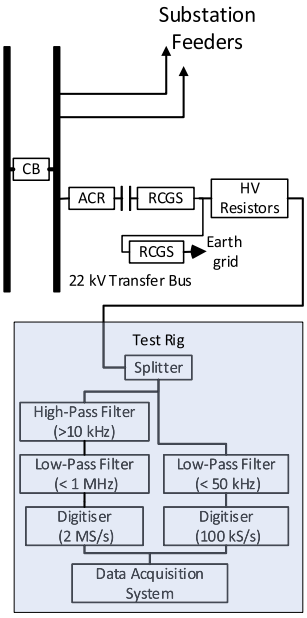

FIGURE 1. Test rig and measurement system.

This work seeks to contribute to literary knowledge by comparing the speed of relative temporal magnitude growth in the LF (DC to 50 kHz) and HF (10 kHz to 1 MHz) current spectrums during the progression of VeHIFs. It is not just sufficient to detect VeHIFs, but also to detect them quickly to minimize the fire risk. Marxsen argues in [16] that detecting earth faults in two seconds can result in a tenfold fire-risk reduction. The utilised methodology relied on analysis of the temporal magnitude growth in the LF and HF components of fault currents (relative to the pre-fault) during the progression of VeHIFs. The key analysis has been undertaken using a dataset of 125 ph-to-e test recordings. A key contribution herein is the protection-speed efficacy contrast of the LF and HF spectrums based on the temporal magnitude growth of components in each spectrum. This focus on the protection-speed efficacy comparison separates the contributions herein from other published disseminations. The results highlight that the HF components hold the real key to the timely detection of VeHIFs with significant lead times over the fault signatures in the LF bands. While acknowledging robustness in the LF components (larger magnitude growths), the HF components should ideally be considered alongside the LF components to combine speed and robustness. The analysis has also revealed that a sampling frequency as large as 1.8 MHz may be needed, when designing high-speed HIF protection applications.

II. LOW AND HIGH FREQUENCY SIGNATURES OF VEGETATION HIGH IMPEDANCE FAULT CURRENTS

The validation dataset features data from staged VeHIFs performed for the '*Vegetation Conduction Ignition Testing*' project [16]. The project focused on sampling and testing of diverse vegetation species in staged HIFs in a test rig (see Figure 1). Ph-to-earth (ph-to-e) fault tests included a

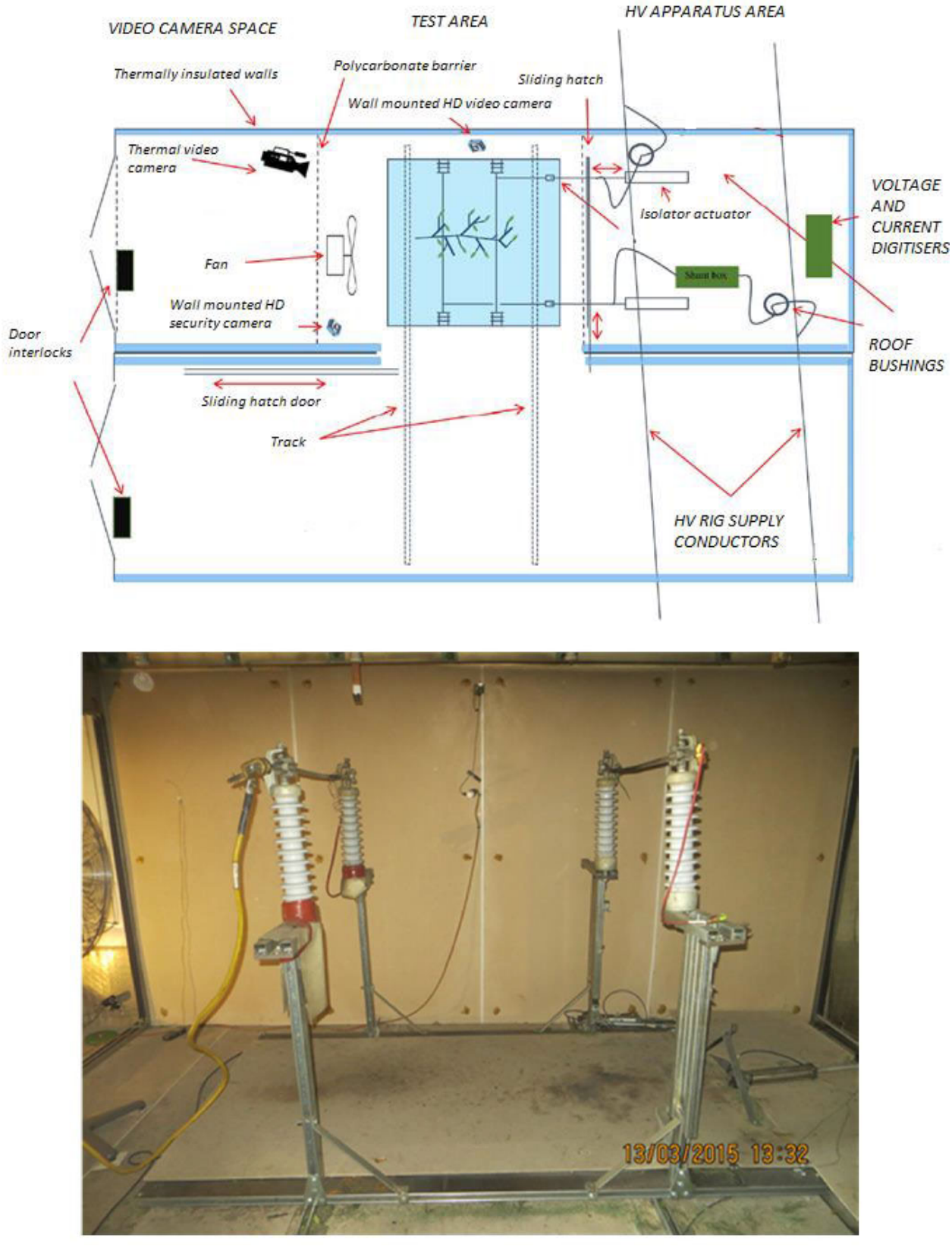

FIGURE 2. Test rig schematic and photographic illustration [16].

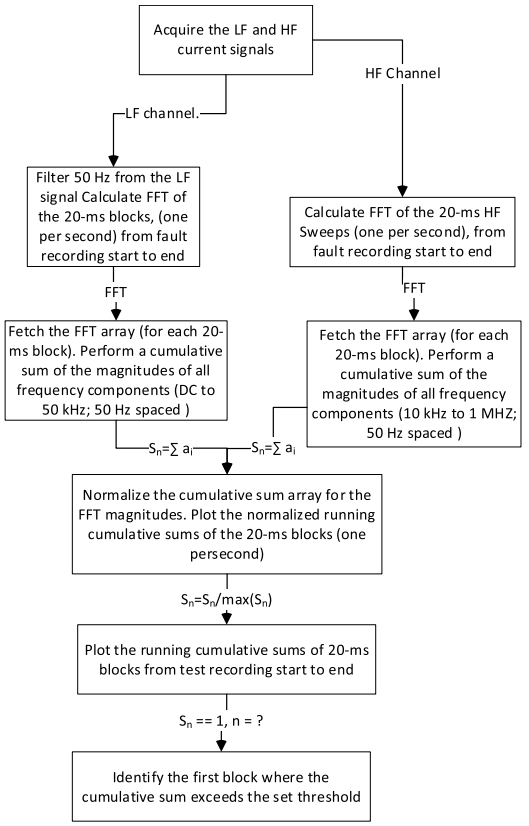

FIGURE 3. Flowchart for the computation and plot of temporal growth magnitudes of LF and HF channels of the fault current.

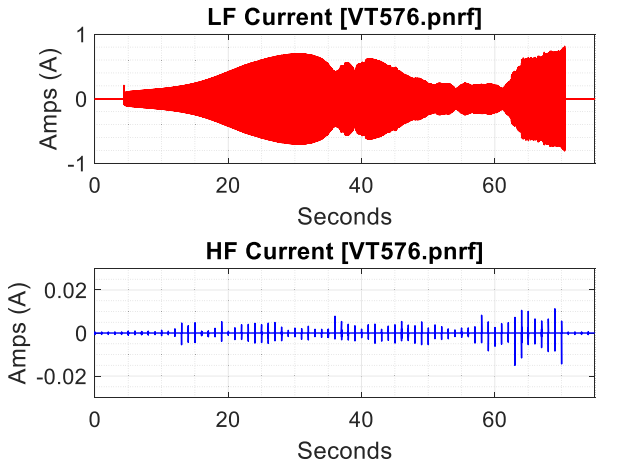

FIGURE 4. LF (top) and HF (bottom) current recordings of a 0.5 A_{rms} limit VeHIF of Eu. Baxteri species (VT576).

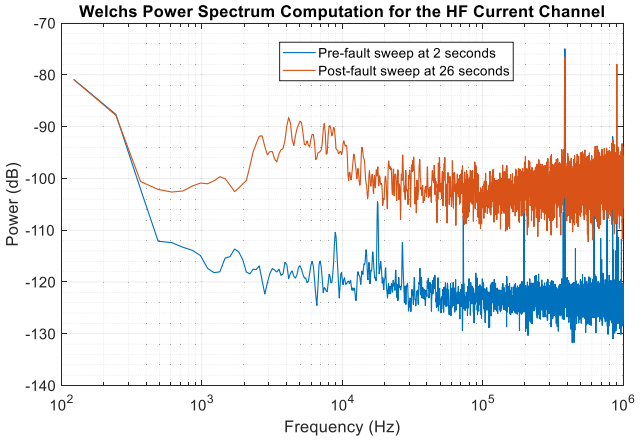

FIGURE 5. Welch's power spectrum estimate for the HF current channel (10 kHz to 1 MHz) at a pre-fault and a post-fault sweeps (VT576).

tree branch laid across two conductors, one energized with 12.7 kV phase voltage and the other earthed. The LF channel (DC to 50 kHz) sampled the fault current continuously with a 100 kSa/s sampling rate. The HF channel (10 kHz to 1 MHz) sampled the fault current with a 2 MSa/s sampling rate in 20-ms sweeps; one sweep every second. 125 fault recordings from [16] have been used in the statistical analysis comprising only the tests that did not result in a flashover and only those that were taken as having resulted a fire in line with the criteria introduced in [16]. Figure 2 shows the test rig schematic and its photographic illustration. The rig supported two parallel conductors with one earthed to operate in the phase-to-earth configuration for staged 'branch touching wire' faults [16].

III. COMPUTATIONAL METHODOLOGY

Figure 3 shows the methodology in the temporal growth comparison. For the LF channel, the 50 Hz component was filtered out, as the key interest was on frequency tones from second harmonic onwards. FFT analysis was then carried out for the 20-ms blocks and linear FFT magnitudes cumulatively added with 50 Hz spaced-out frequency tones. A similar process was repeated for the HF channel sweeps and the FFT array cumulatively added for the 10 kHz to 1 MHz range with. The data was parsed through for each channel identifying the times when the temporal growth exceeded the given threshold. This knowledge was used for the statistical comparison of the protection-speed efficacy of the two spectra. Statistical tools such as the mean, max and standard deviation are used in interpreting the results. This includes the 'leading indicator' comparison of LF & HF spectra, where authors sought to identify patterns that could be generalised, e.g. HF indicators are generally faster than LF indicators. The analysis then sought to identify the lead time comparison of the indicators.

IV. PSD AND TEMPORAL GROWTH ANALYSIS OF LF AND HF SPECTRA DURING TWO SAMPLE FAULTS

Figure 4 shows the LF and HF channel recordings during one example ph-to-e vegetation test (Eu. Baxteri species) labelled as 'VT576'. As illustrated, the LF current was continuously recorded. In this work, the HF channel's 20-ms sweeps were amalgamated enabling linked visualization of the LF and HF events in the time-domain. The HF channel shows the amalgamation of the sweep recordings where 0.98-s of appended zeros tail each 20-ms sweep. The test had a current limit and it was terminated once the fault current reached 0.5 A_{rms}. Figure 5 and Figure 6 compare the Power Spectral Density (PSD) of the LF and HF channels using pre-fault and post-fault sweeps from VT576. Figure 5 compares the

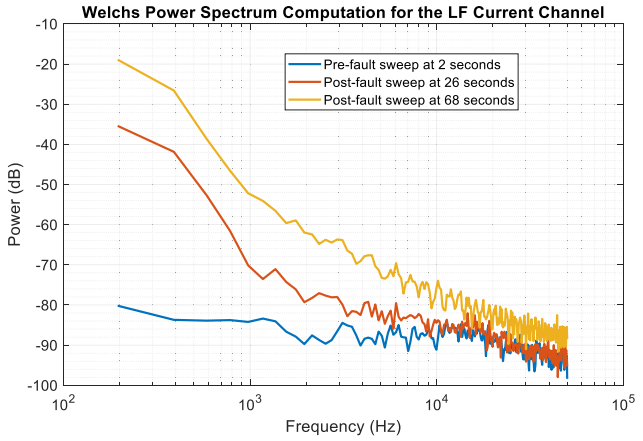

FIGURE 6. Comparison of Welch's power spectrum estimate for the LF current at three intervals: a pre-fault sweep and two post-fault sweeps.

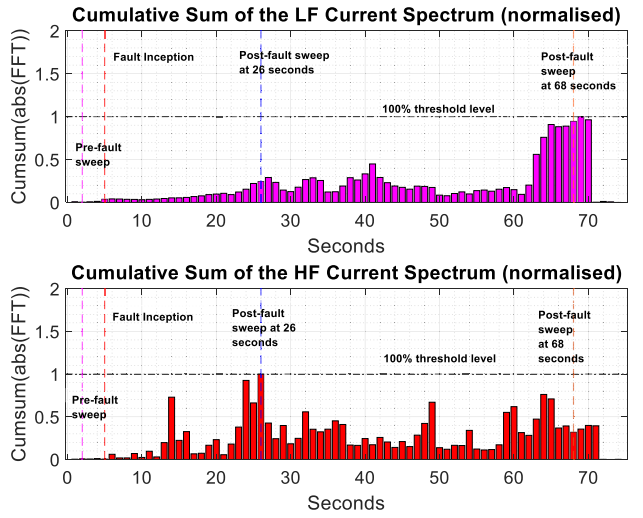

FIGURE 7. Temporal spectral magnitude growth comparison of the LF and HF spectrums from fault start to fault end for test VT576.

HF PSD of a pre-fault sweep (2 seconds into the recording) and a post-fault sweep (26 seconds into the recording). The analysis clearly shows how the HIF affects the HF spectrum of the measured current signal. As illustrated, an overall lift in the spectrum was observed particularly for frequencies above 300 Hz. Some peaks, greater than 400 kHz, are attributed to the local AM radio stations and EMI sources. Figure 6 presents a similar PSD analysis of the LF channel for one pre-fault sweep and two post-faults sweeps. A significant observation in Figure 6 is how the overall lift in the PSD spectrum gets larger towards the end of the fault (68 s into the recording) as compared to the mid-fault sweep (26 s into the recording). This observation revealed that for VT576, the temporal growth in the LF components was highest only at the end of the fault.

For temporal growth comparison, the cumulative sums of 20-ms window Fast Fourier Transform (FFT) magnitudes (area under the frequency domain plot, linear scale) were normalized to their post-fault maximum and plotted as in Figure 7. The normalization process enabled to compare the

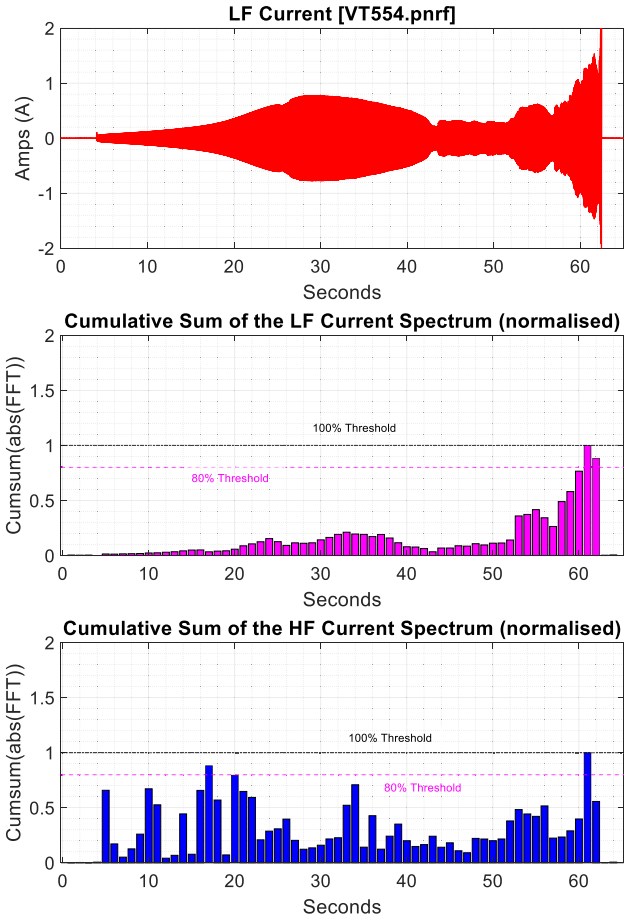

FIGURE 8. Temporal spectral magnitude growth comparison of the LF and HF spectrums from fault start to fault end for test VT554.

speed of growth in the LF and HF components, rather than a focus on the size of growth in the two spectrums. A clear observation from the LF spectral analysis (see Figure 7) is that its temporal growth reached its highest level at the end of the fault akin to the observation made in Figure 6. On the contrary, for the 10 kHz to 1 MHz channel, the relative temporal growth reached its max 100 % level only after 26 s into the fault. Most classifiers seek to compare pre-fault and post-fault levels in the classification of faults. The amount of deviation of the LF and HF components from their respective no-fault levels is surely very critical in terms of security, but the speed of growth should also be considered in designing for fast fault clearance. While the results in Figure 7 do not imply a 2 s guaranteed response time as recommended in [16], it shows that a much faster protection speed can potentially be achieved by integrating the HF components into the overall scheme.

Reaching conclusions after the analysis of just one single test is certainy not sufficient for generalising concepts. For this purpuse, a second temporal growth analysis is presented for VT554 (Eu. Viminalis species, 1 A_{rms} current limit) in Figure 8. The normalised values have been plotted to compare the level of temporal growth (relative to the pre-fault levels) that the fault causes in each distinct spectrum. The

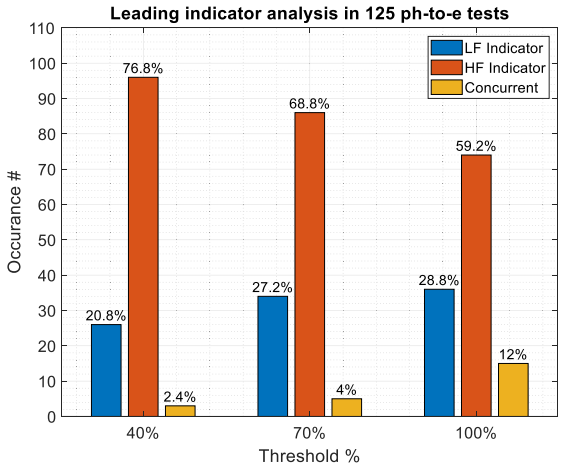

FIGURE 9. Leading indicator comparison of LF and HF spectral temporal growth indicators for different thresholds (125 ph-to-e tests).

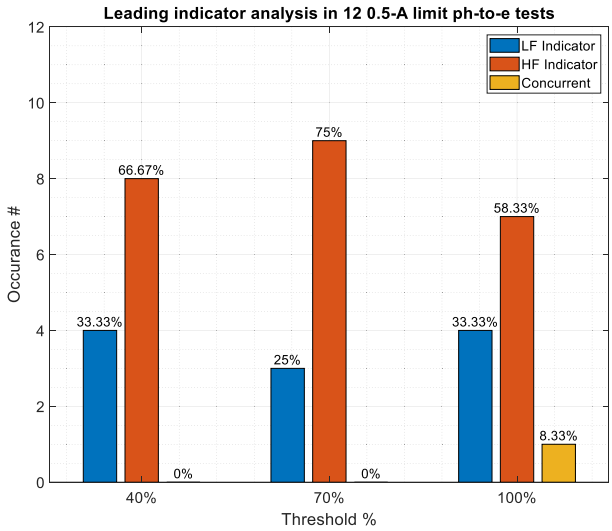

FIGURE 10. Leading indicator comparison of LF & HF spectral temporal growth indicators for different thresholds (12 0.5-A limit ph-to-e tests).

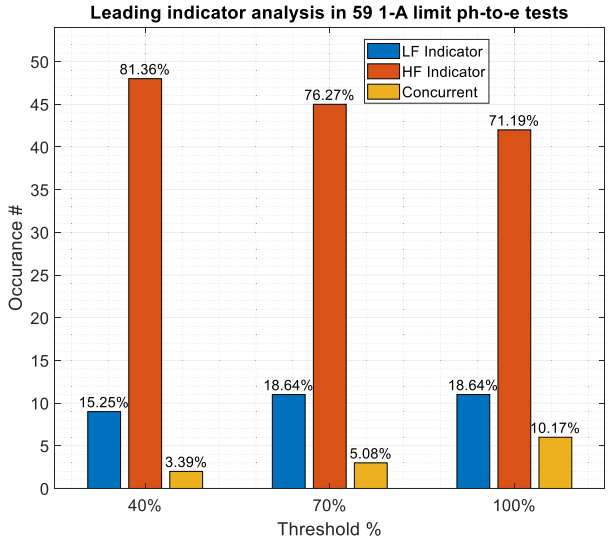

FIGURE 11. Leading indicator comparison of LF & HF spectral temporal growth indicators for different thresholds (59 1-A limit ph-to-e tests).

100 % and 80 % threshold levels have been highlighted in Figure 8. The 'threshold' represents the target trigger level with respect to the post-fault maximum of the cumulative sum. In this test, one observation was that both features would have triggered the 100 % thereshold violation at sixty one seconds into the fault. However, when the threshold level was reduced to 80 %, the HF current spectum triggered a threshold level violation only after seventeen seconds as compared to sixty one seconds for the case of the LF spectrum. This second analysis confirms the hypothesis that the temporal growth in the HF components is likely to occur faster, but has highlighted that the set threshold level also plays a critical factor. This has prompted the need to further increase the test size of the analysed fault data such that more generalised assertions could be made. For this purpuse, 125 ph-to-e fault tests have been analysed and the comparative results are presented in the following section.

V. ANALYSIS OF TEMPORAL GROWTH SPEED IN THE LF AND HF INDICATORS USING A LARGE DATASET

This section presents the temporal growth analysis of 125 ph-to-e fault recordings. The 'lead indicator' analysis targets to identify the indicator that reaches the set threshold level prior to the other. The term 'LF indicator' describes the frequency components from DC to 50 kHz, while the term 'HF indicator' refers to the components in the 10 kHz to 1 MHz range. The dataset comprises twelve 0.5-A current limit, fifty-nine 1-A current limit and fifty-two 2-A current limit tests (excluding tests that resulted in a flashover and only including those that were taken as having resulted a fire as per [16]). Figure 9 shows the performance of the two indicators in terms of their lead statuses for the thresholds of 40 %, 70 % and 100 %. For the 40 % level, the LF spectrum was the lead indicator in 26 out of 125 tests (20.8 %) and the HF spectrum led in 96 out of 125 tests (76.8 %). In 3 tests (2.4 %), both indicators concurrently reached the threshold.

When the threshold was increased, the lead percentage of the LF indicator increased, while the lead percentage of the HF indicator decreased. Another observation is that there was higher number of concurrent finishes, when the threshold was increased. The overall lead-indicator breakdown for the two indicators was 68.2 % for the HF spectrum, and 25.6 % for the LF spectrum (after averaging the three threshold results). Figures 10 to 12 show the leading indicator analysis for the 0.5-A, 1-A and 2-A current limit categories consecutively. Few notable observations are as follows: Principally, the least number of concurrent trigger occurrences was observed for the 0.5-A limit category. Secondly, the separation in between the percentages of the two indicators was largest for the 40 % threshold category of the 1-A limit tests. Conversely, the smallest separation occurred in the 2-A limit test group. In the 0.5-A limit group of tests, the HF indicator performed better at the 70 % threshold than it did at the 40 % threshold. The presented results support the key recommendation herein that HF components should ideally be considered in

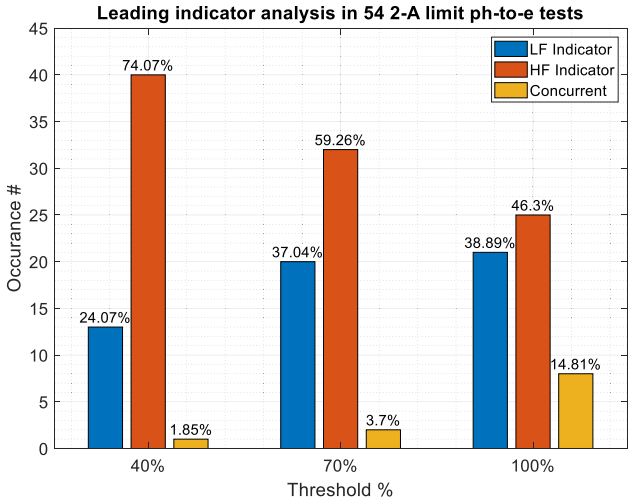

FIGURE 12. Leading indicator comparison of LF & HF spectral temporal growth indicators for different thresholds (54 2-A limit ph-to-e tests).

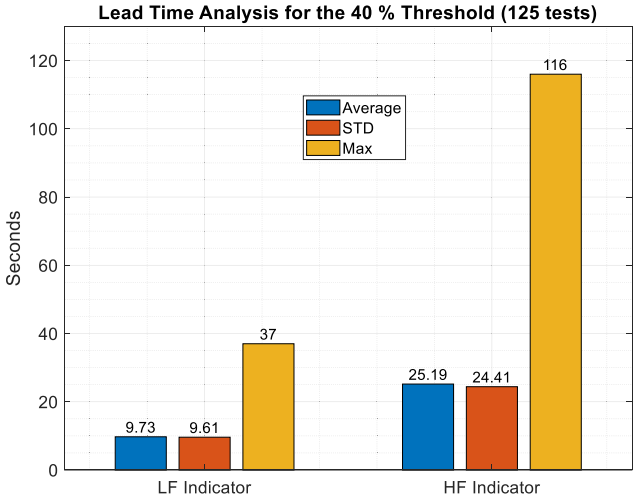

FIGURE 13. Statistical analysis of the lead-times of the two indicators in 125 ph-to-e tests (40 % threshold).

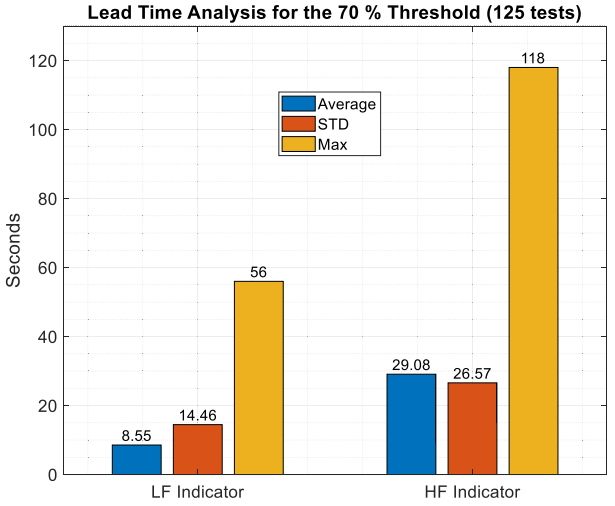

FIGURE 14. Statistical analysis of the lead-time difference of the two indicators in 125 ph-to-e tests (70 % threshold).

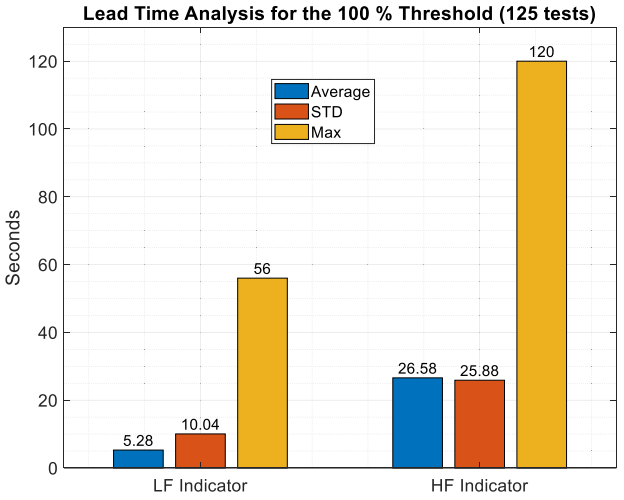

FIGURE 15. Statistical analysis of the lead-times of the two indicators in 125 ph-to-e tests (100 % threshold).

any protection scheme, where fast action times are desirable. The proceeding lead-time analysis will further strengthen this hypothesis.

VI. LEAD TIME COMPARISON OF THE INDICATORS

Figures 13, 14, and 15 analyse the lead-time (in seconds) of the two indicators, for the same dataset of 125 ph-to-e tests (for three different normalised magnitude thresholds). The lead-time measures how many seconds a particular indicator reaches the set threshold level prior to the other indicator. For example, for the VT576 test in Figure 7 (100 % threshold case), the lead time of the HF current spectrum was 42 s as it triggered a 100 % threshold level violation at 26 s into the recording, while the LF indicator triggered the same at 68 s into the recording. For the VT554 example (see Figure 8), the lead-time was zero for the 100 % case, but the HF indicator led by 44 s in the 80 % threshold level case. Thus, a small reduction in the threshold level could potentially make a very significant difference in the lead-time of HF components.

For the 40 % threshold case, in 26 out of 125 tests (20.8 %), the LF indicator was faster than the HF indicator with an average lead-time of 9.73 s, a standard deviation (STD) of 9.61 s and a maximum lead-time of 37 s. On the other hand, the HF indicator was faster than the LF indicator with an average lead-time of 25.19 s, a STD of 24.41 s, and a maximum lead-time of 116 s. The analysis therefore shows that the HF indicator was faster than the LF indicator in a larger number of tests with a much larger lead-time margin. In contrast, the LF indicator was faster in fewer tests with a smaller margin of lead-time. Similar observations can be observed for the 70 % and 100 % threshold cases. Across all threshold settings, the HF indicator had an average lead-time of 26.95 s and the LF indicator had an average lead-time of 7.85 s (after averaging the three individual threshold results).

The significantly high standard deviation in all threshold settings point to the fact that the lead-time values are very spread out and not clustered around the mean. This can

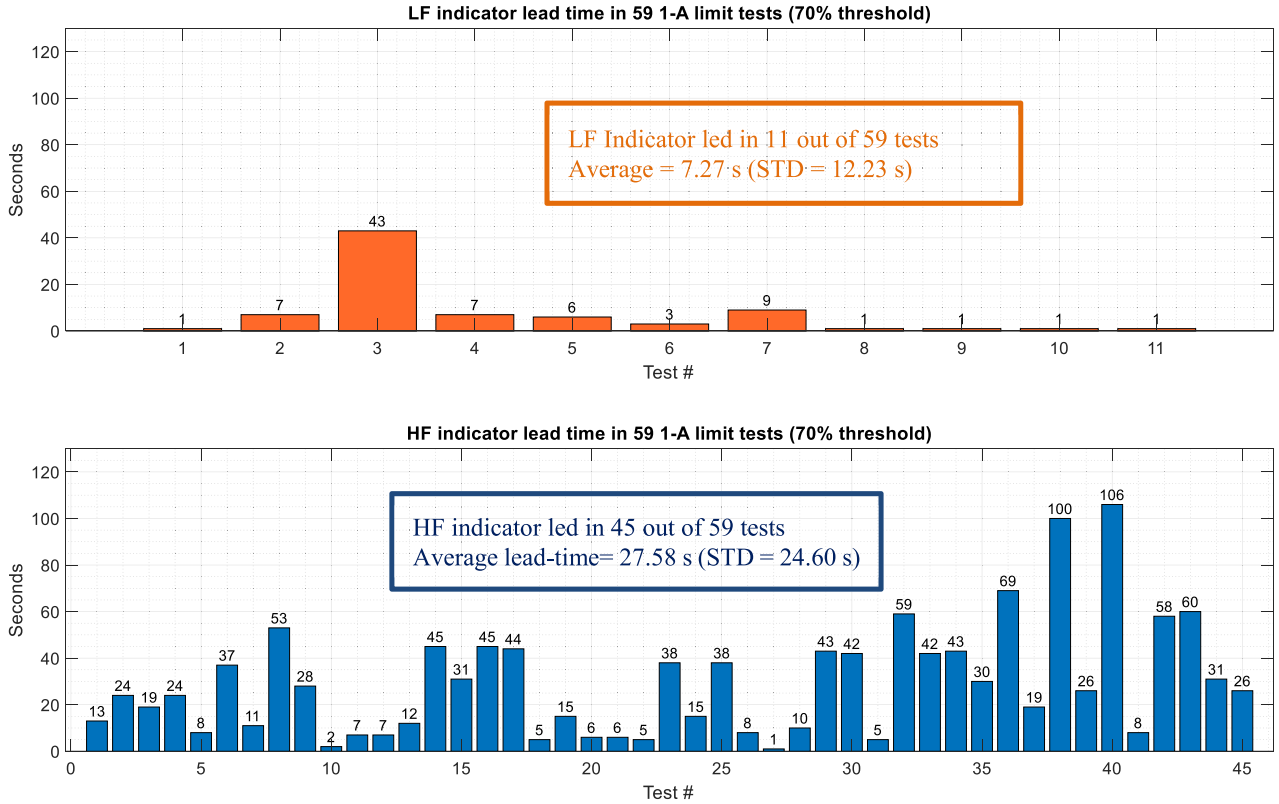

FIGURE 16. Lead time comparison of the LF and HF spectra in fifty-nine 1-A limit tests (70 % threshold).

be better visualised from Figures 16 and 17, which provide the distribution of the lead times for two selected analysis cases: (i) 59 1-A limit tests (70 % threshold) and (ii) 54 2-A limit tests (100 % threshold).

As shown in Figure 16, the LF indicator led in 11 out of 59 (18.64 %) tests for the 1-A current limit tests. Its largest lead-time was 43 s, but all other lead times were smaller than 10 s. Conversely, the HF indicator not only had the lead in 45 out of 59 tests (76.27 %), but also performed better with a higher lead-time margin.

For the fifty-four 2-A limit 100 % threshold tests (see Figure 17), the percentage breakdown was 38.89 % and 46.3 % for the LF and HF indicators successively. These relatively close percentages do not reflect the true strength of the HF spectrum until the lead times are analysed. As in Figure 17, the HF indicator led decisively in most of the 25 tests with a lead-time average of 30.84 s, whereas the LF indicator had only a one-second lead in 12 out of 21 tests and an overall lead-time average of 5 s. This analysis has further validated the high speed of temporal growth in HF components. Considering that higher sampling rate signifies higher costs, the following section attempts to identify the optimum sampling rate for an upper hand in providing a fast response.

VII. HIGH FREQUENCY BAND ANALYSIS FOR OPTIMAL SAMPLING RATE

This section divides the HF spectrum into ten distinct bands and presents an analysis of the temporal growth comparison of the ten bands using the same dataset. The key objective is to identify the leading HF bands with the fastest growth. Figure 18 shows the LF and HF channel recordings during a 2-A limit VeHIF test (F. Angustifoli) labelled as 'VT943'. For analysing the temporal relative growth in various bands (see Figure 19) of the HF spectrum, the cumulative sums of 20-ms window FFT magnitudes (area under the frequency domain plot, linear scale) were normalized to their largest post-fault values and plotted in Figure 19.

While acknowledging that the overall magnitude of fault signature contribution will be different in each band (e.g. larger in the lower bands), the work presented herein aims to identify how quickly the fault current contribution reaches its maximum in each band. This is irrespective of the magnitude of the fault current contributions in the bands. For example, for the case of VT943, the maximum fault current contribution in the first band (50 kHz to 100 kHz) was 45 mA, but this level was breached only after 179 s into the recording. On the other hand, the maximum fault current contribution in the 700 kHz to 800 kHz band was 2.8 mA, but this level was breached only 60 s into the fault. While authors recognize the robustness (larger signal magnitudes) of the lower HF bands, the results show that they have slower temporal growth, when compared to the higher bands. One key recommendation is that in designing a HIF protection scheme, where speed is as critical as robustness, the upper HF band fault signatures should potentially be considered alongside the lower frequency components. For a 100 % threshold setting, the

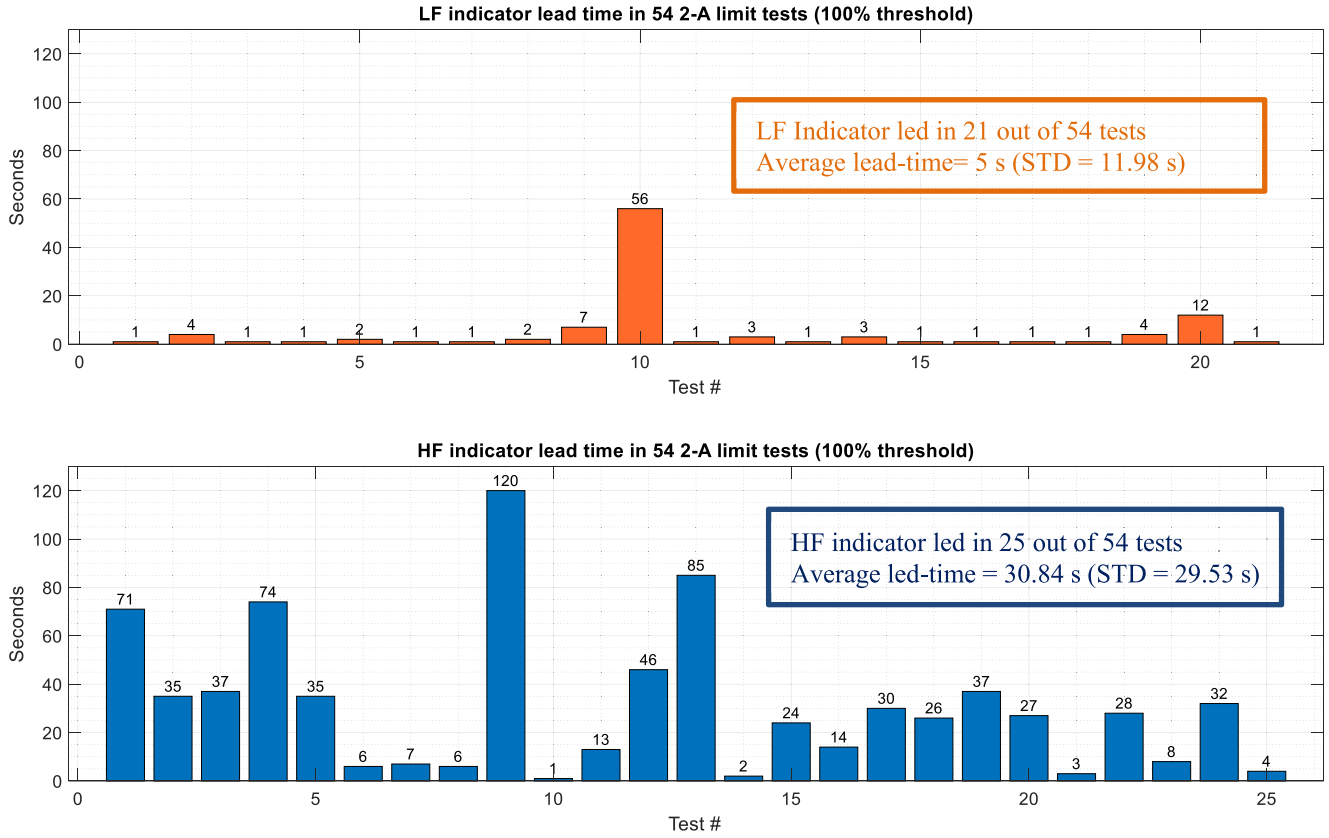

FIGURE 17. Lead time comparison of the LF and HF spectra in fifty-four 2-A limit tests (100 % threshold).

800 kHz to 900 kHz band had the fastest growth, in the case of the test VT943 (see Figure 19). The 50 kHz to 100 kHz band had the slowest growth despite being the band with the largest fault signature magnitude.

The hypothesis that the upper HF bands contain fast fault current signature growth has been verified using 125 ph-to-e fault recordings. Figures 20 and 21 show the comparison of ten HF spectral bands for temporal fault signature growth for the 40 % and 70 % threshold levels. As shown in Figures 20 and 21, the 800 kHz to 900 kHz band (the ninth band) had the fastest growth in 87 out of 125 tests (40 % threshold) and 82 out of 125 tests (70 % threshold). In both threshold cases, the tenth band (900 to 1000 kHz) performed poorer than the ninth band, potentially signifying that the 1.8 MHz sampling rate may indeed be the optimal rate required, when designing HIF protection applications to combine speed and robustness in clearing faults.

When the threshold was increased to 100 %, the 700 kHz to 800 kHz band had the fastest growth in 85 out of 125 tests as in Figure 22. The 800 to 900 kHz band (9^{th} band) had the second best fastest growth performance in 82 out of 125 tests (65.6 %). The analysis of results from all three figures imply that the 9^{th} band had a three-threshold average 66.93 % lead in the temporal growth of fault signatures. Given that the sampling rate of recordings was 2 MSa/s during the test days, frequencies higher than 1 MHz could not be adeptly evaluated. Table 1 lists the various average 'time

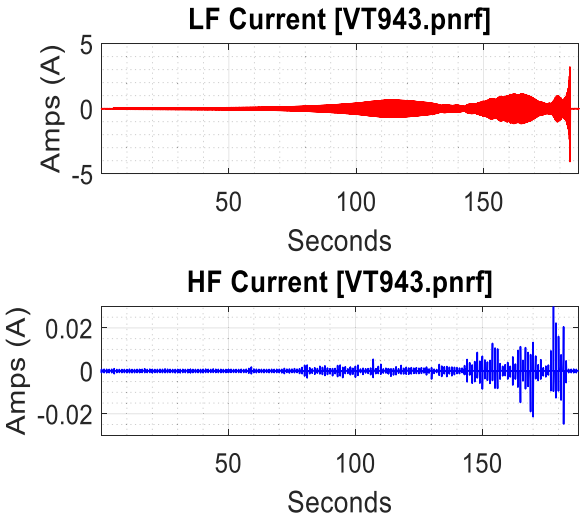

FIGURE 18. LF (top) and HF (bottom) current recordings of a 2 A_{rms} limit VeHIF of F. Angustifolia species (VT943).

to the threshold' metrics of the various HF bands for the three different threshold settings. In essence, the 'time to the threshold' measures the amount of seconds each HF band took (from recording start onwards) to reach the set threshold. Table 2 presents the overall averages. As anticipated, Band 9 had the smallest 'time to the threshold' value. An even more interesting observation is the sharp drop in the durations,

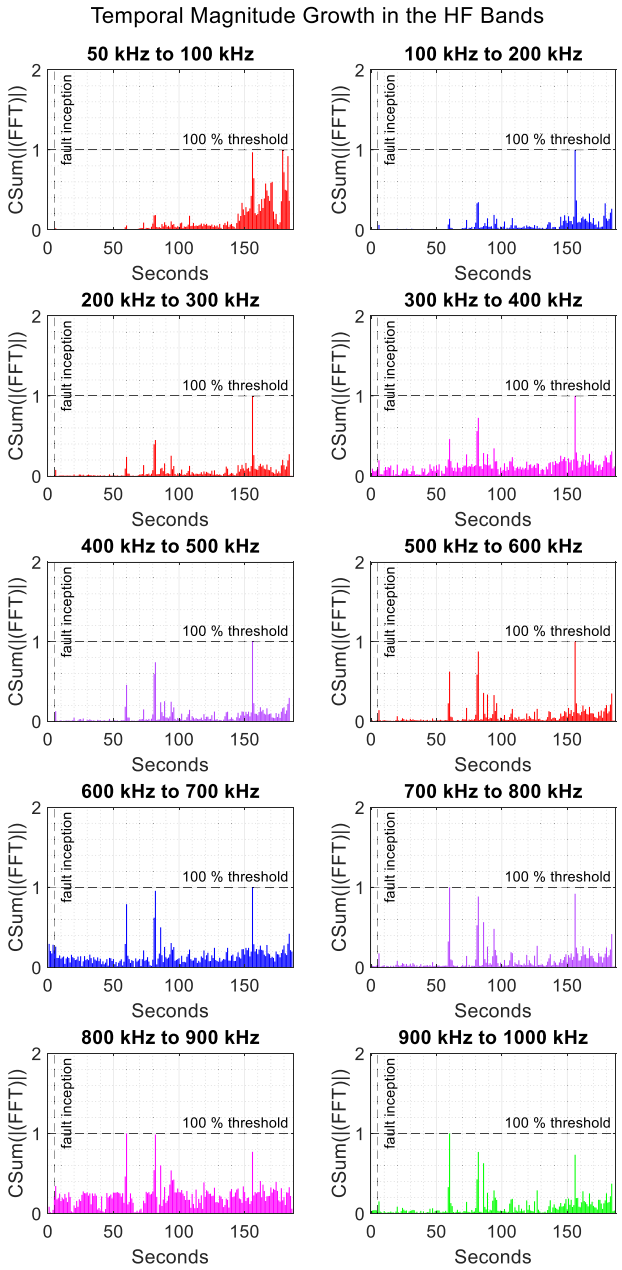

FIGURE 19. Temporal spectral magnitude growth comparison of ten HF bands (VT943).

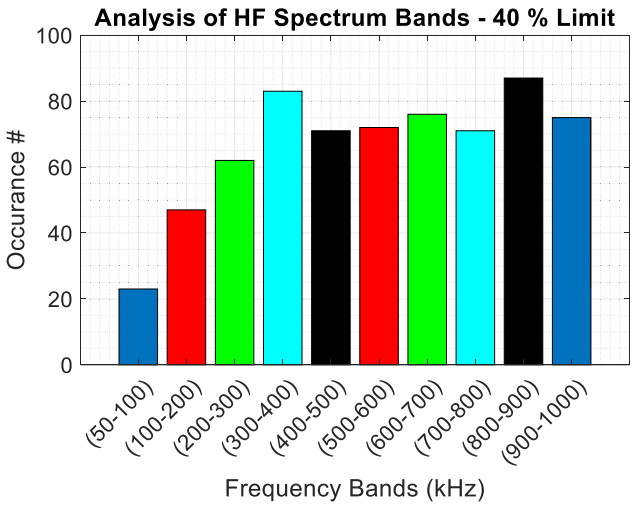

FIGURE 20. Leading indicator comparison of ten HF spectral bands for temporal growth of fault signatures (40 % normalised threshold limit).

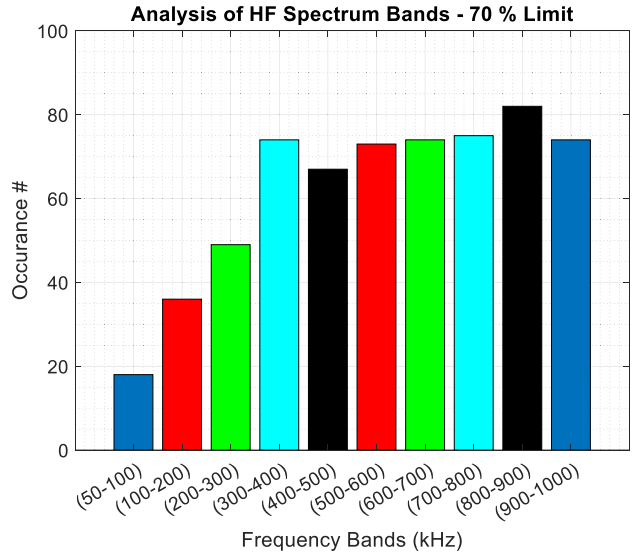

FIGURE 21. Leading indicator comparison of ten HF spectral bands for temporal growth of fault signatures (70 % normalised threshold limit).

after the first three bands. As shown, the temporal growth gets faster as the frequency band increases, but the growth in the first two bands is explicitly slower than the remaining bands. While the Bands 4 to 10 had relatively close 'time to the threshold' durations, those in the first two bands were distinctly slower. This is a further justification towards the key recommendation in this paper that HF components should preferably be utilised together with the LF indicators for a fast response to VeHIF events.

VIII. COMPARISON OF HIFs WITH DISTURBANCES

LF and HF spectra indicators could potentially classify other disturbances such as capacitor bank and asynchronous machine (AS) switching or starting a Variable-Speed Drive (VSD) controlled AC motor. It is therefore critical to distinguish such disturbances from HIFs for not leading to false positive events. In this section, authors present the application of the same temporal growth analysis for the above-mentioned disturbances. In simulating the transient currents during the switching of a capacitor bank, a 600-kVAr 3-phase capacitor bank has been modelled in a 5-bus radial 22-kV feeder. In the case of the asynchronous machine, a 10 HP squirrel-cage induction machine is connected to the 22-kV feeder through a step-down transformer. The third modelled disturbance is a low voltage VSD controlled AC motor also connected to the feeder through a step-down transformer. In the temporal growth analysis of the disturbances, 20-ms sweeps (one per every 0.1 s) has been used. In all three cases, the switching takes place at the 0.5 s.

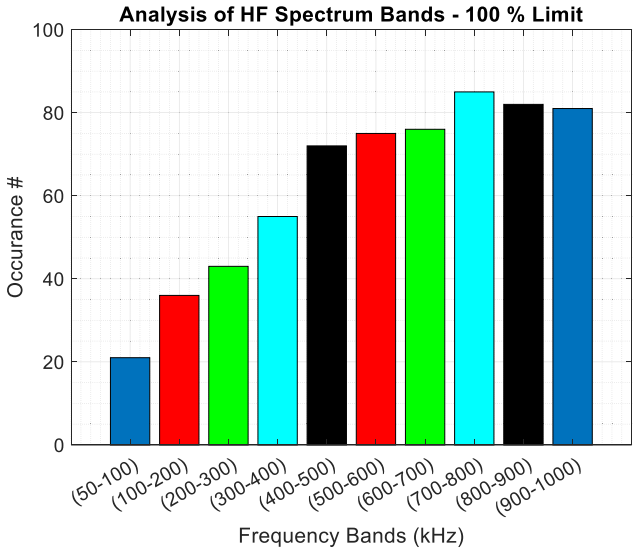

FIGURE 22. Leading indicator comparison of ten HF spectral bands for temporal growth of fault signatures (100 % normalised threshold limit).

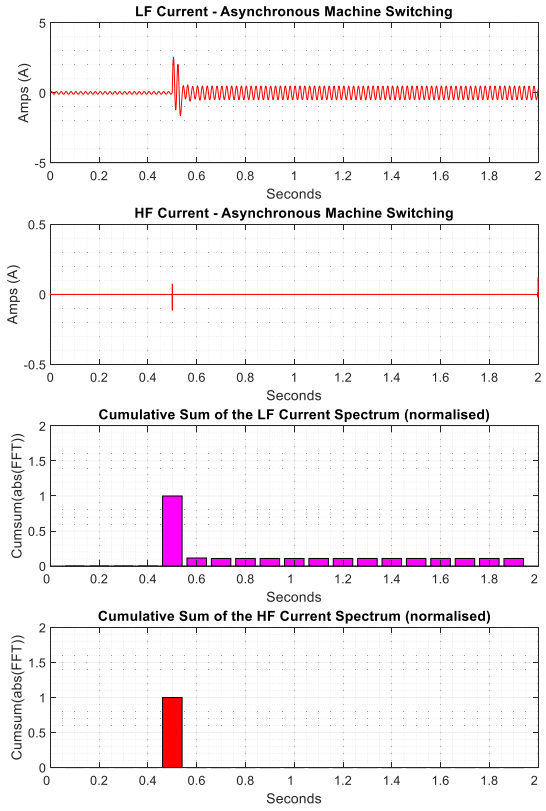

FIGURE 23. Temporal growth analysis of LF and HF spectra components during asynchronous machine switching.

Figure 23 shows the analysis of the disturbance current due to switching of the AS machine. As shown, there is a sudden increase in both the LF and HF components post switching of the capacitor. However, these either die down or stabilize quickly. A similar observation can be seen in the case of the capacitor bank switching (see Figure 24). For the VSD controlled motor (see Figure 25), this stabilisation (LF indicator) and removal (HF indicator) lasts slightly longer, but cannot replicate the unstable HIF current behaviour.

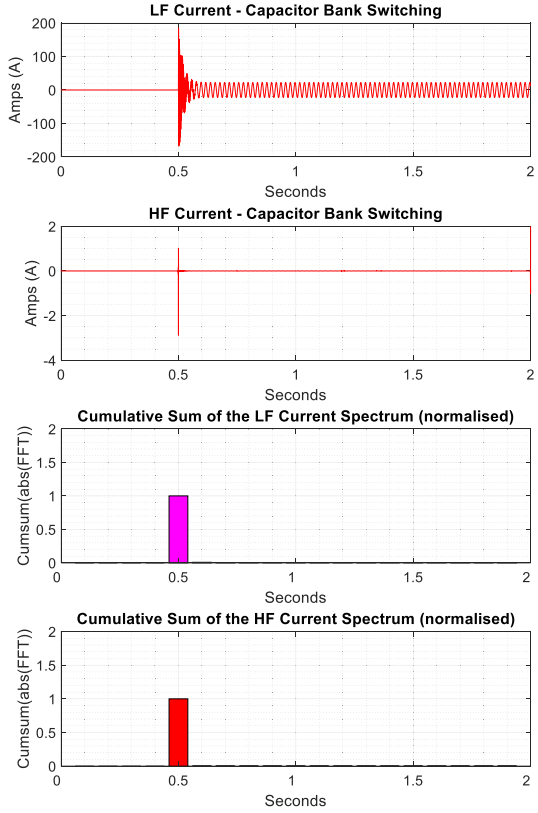

FIGURE 24. Temporal growth analysis of LF and HF spectra components during capacitor switching.

TABLE 1. Average lead time comparison of ten high frequency bands for various threshold levels.

Band	Frequency (kHZ)	100 % threshold	70 % threshold	40 % threshold
1	50 – 100	59.608 s	52.576 s	40.832 s
2	100 – 200	54.352 s	47.256 s	32.496 s
3	200 – 300	49.4 s	40.072 s	26.24 s
4	300 – 400	45.192 s	33.232 s	22.8 s
5	400 – 500	42.216 s	33.208 s	24.992 s
6	500 – 600	40.72 s	32.264 s	23.544 s
7	600 – 700	38.96 s	31.632 s	23.544 s
8	700 – 800	36.976 s	31.232 s	24.072 s
9	800 – 900	37.288 s	29.896 s	21.512 s
10	900 – 1000	37.4 s	31.008 s	22.968 s

In comparing the disturbances (presented in Figures 23 to 25) to the HIF currents, significant differences can be observed. HIF current LF and HF signatures are long lasting, unstable and very random. In the case of the analysed disturbances, disturbance signatures are short-lived and instant with the core of the LF and HF signatures being present during the few ms of the switching activity. These disturbances certainly cause LF and HF signatures, but the short-lived nature of these is the key to discriminating them from HIFs. Authors have always argued for the need to achieve a balance between speed and security of a protection scheme, and the short-lived nature of the signatures of these disturbances show that they can easily be discriminated from

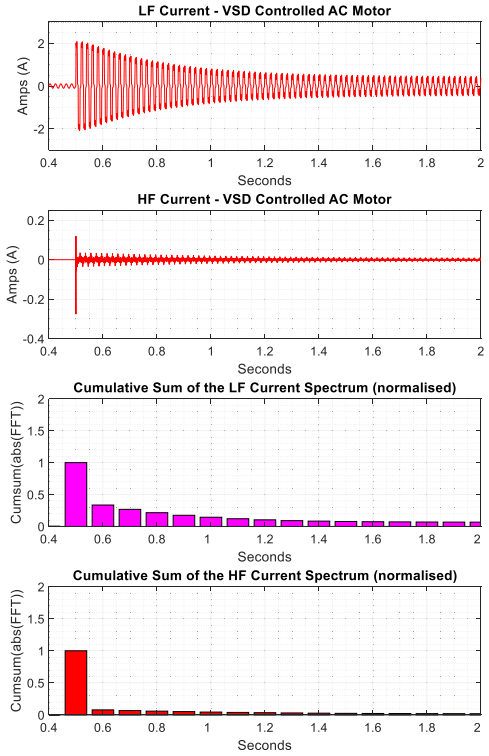

FIGURE 25. Temporal growth analysis of LF and HF spectra components during VSD controlled AC motor switching.

HIFs by allowing an extra second or two. Based on the analysis provided in [16], while it is true that detecting earth faults in 2 seconds can result in a tenfold fire-risk reduction, it should also be not undermined that a vegetation sample needs to experience a sustained exposure to conduction (see [17] for further analysis on the matter) before it advances into progressive charring. In a bush-fire, ember formation (due to charring) and falling of these to the forest-bed really initiate the spread of the fire. The former analysis in [17] on stages of vegetation ignition development suggest that in most cases, there will be sufficient time (before current conduction results in progressive charring and ember formation) in discriminating a disturbance from a HIF relying on the fact that VeHIF signatures would be sustained far longer than that experienced during other switching disturbances.

IX. DISCUSSION OF RESULTS

The results presented suggest that a sampling frequency, as large as 1.8 MHz, is ideally essential in feeder protection applications requiring fast HIF detection speeds. This key conclusion is well aligned with the results presented in [18], where the efficacy of an even higher sampling rate of 250 MSa/s was validated for capturing HF transient disturbances. In comparison, the 'F60 Feeder Protection System' (a relay marketed for HIF detection capability) has a sampling rate of 3.2 kSa/s (in a 50-Hz system) [19]. Research by another protection relay manufacturer recommends [20] a sample rate of 32 samples per cycle (1.6 kSa/s in a 50-Hz system). In the HF band analysis undertaken in this work,

TABLE 2. Overall average lead time of ten high frequency bands.

Band	Frequency (kHZ)	Lead Time
1	50 – 100	51.01 s
2	100 – 200	44.70 s
3	200 – 300	38.57 s
4	300 – 400	33.74 s
5	400 – 500	33.47 s
6	500 – 600	32.18 s
7	600 – 700	31.38 s
8	700 – 800	30.76 s
9	800 – 900	29.57 s
10	900 – 1000	30.46 s

the 700 kHz to 800 kHz and the 800 kHz to 900 kHz bands had the fastest growth to their post-fault signature maxima in a large dataset of HIF fault recordings. This is notable because in a protection method (using any one of the artificial intelligence techniques), where pre and post fault signatures levels are monitored, the frequency tones in these two bands will show the quickest deviation from their pre-fault normal levels (assuming adoption of a margin of safety). Our analysis of a set of network disturbances (such as capacitor switching) has shown that the LF and HF signatures associated with these events often dissipate after 1 s. This suggests that a method, which checks for the continuity of signatures beyond the first second of signature upsurge, could successfully discriminate these disturbances from true HIFs.

X. CONCLUSION

This paper has presented a study on the protection-speed efficacy of the LF (DC to 50 kHz) and HF (10 kHz to 1 MHz) fault signatures based on the analysis of the temporal growth speeds in each spectrum. The analysis was undertaken using a dataset of 125 ph-to-e test recordings to derive statistically meaningful recommendations. Moving cumulative sums of 20-ms window FFT magnitudes were calculated, normalised and plotted for each spectrum. Normalization enabled to compare the speed of growth in the two spectrums, instead of a magnitude based comparison. The temporal growth analysis and contrast of the LF and HF spectrums was later undertaken against three levels of threshold, representing the target growth trigger levels with respect to the post-fault maximum of the cumulative sum. While acknowledging that the overall magnitude of fault signatures are higher in lower frequency bands, the results show that HF components hold the real key to fast detection of VeHIFs with significant lead times over the fault signatures in the LF spectrum.

Growth in the HF spectral components was faster in 68.2 % (the overall average of three categories of threshold levels) of the 125 ph-to-e tests with a higher average lead-time of 26.95 s. The LF indicator was faster in 25.6 % of the tests with a smaller average lead-time margin of 7.85 s. When the threshold level was increased, a higher number of concurrent finishes was observed. The lead percentage of the LF indicator increased and that of the HF indicator decreased, when the threshold level was increased. The work presented also

sought to analyse the temporal growth of fault signatures in the HF spectrum using ten distinct bands. The ninth band, from 800 to 900 kHz, had an average 66.93 % lead in the temporal growth of signatures. The bands below or higher than the ninth band had lower averages. The temporal growth speed of HIF signatures was observed to get faster as the frequency band increased. The temporal growth in the first two bands (50 kHz to 100 kHz, 100 kHz to 200 kHz) was explicitly slower than the remaining bands. Accordingly, the optimum sampling rate has been identified as 1.8 MHz for an upper hand in designing protection schemes, where the speed of protection is as critical as robustness. The key study outcome had validated that the HF components should ideally be considered alongside the LF components to combine speed and robustness in HIF detection applications.

REFERENCES

[1] S. Wang and P. Dehghanian, "On the use of artificial intelligence for high impedance fault detection and electrical safety," *IEEE Trans. Ind. Appl.*, vol. 56, no. 6, pp. 7208–7216, Nov. 2020, doi: 10.1109/TIA.2020.3017698.

[2] V. Torres-Garcia, D. Guillen, J. Olveres, B. Escalante-Ramirez, and J. R. Rodriguez-Rodriguez, "Modelling of high impedance faults in distribution systems and validation based on multiresolution techniques," *Comput. Electr. Eng.*, vol. 83, May 2020, Art. no. 106576, doi: 10.1016/j.compeleceng.2020.106576.

[3] Y. Chen, J. Yin, Z. Li, and R. Wei, "Single-line-to-ground fault location in resonant grounded systems based on fault distortions," *IEEE Access*, vol. 9, pp. 34325–34337, 2021, doi: 10.1109/ACCESS.2021.3061211.

[4] H. Teimourzadeh, A. Moradzadeh, M. Shoaran, B. Mohammadi-Ivatloo, and R. Razzaghi, "High impedance single-phase faults diagnosis in transmission lines via deep reinforcement learning of transfer functions," *IEEE Access*, vol. 9, pp. 15796–15809, 2021, doi: 10.1109/ACCESS.2021.3051411.

[5] F. Mumtaz, K. Imran, S. B. A. Bukhari, K. K. Mehmood, A. Abusorrah, M. A. Shah, and S. A. A. Kazmi, "A Kalman filter-based protection strategy for microgrids," *IEEE Access*, vol. 10, pp. 73243–73256, 2022, doi: 10.1109/ACCESS.2022.3190078.

[6] Q. Cui, K. El-Arroudi, and Y. Weng, "A feature selection method for high impedance fault detection," *IEEE Trans. Power Del.*, vol. 34, no. 3, pp. 1203–1215, Jun. 2019, doi: 10.1109/TPWRD.2019.2901634.

[7] E. M. Lima, R. de Almeida Coelho, N. S. D. Brito, and B. Alencar de Souza, "High impedance fault detection based on stockwell transform," in *Proc. IEEE PES Transmiss. Distrib. Conf. Exhib. Latin Amer. (TD-LA)*, Sep. 2018, pp. 1–5, doi: 10.1109/TDC-LA.2018.8511711.

[8] S. Gautam and S. M. Brahma, "Detection of high impedance fault in power distribution systems using mathematical morphology," *IEEE Trans. Power Syst.*, vol. 28, no. 2, pp. 1226–1234, May 2013, doi: 10.1109/TPWRS.2012.2215630.

[9] B. M. Aucoin and B. D. Russell, "Distribution high impedance fault detection utilizing high frequency current components," *IEEE Power Eng. Rev.*, vol. PER-2, no. 6, pp. 46–47, Jun. 1982, doi: 10.1109/MPER.1982.5521003.

[10] B. Aucoin and B. Russell, "Distribution high impedance fault detection utilizing high frequency current components," *IEEE Trans. Power App. Syst.*, vol. PAS-101, no. 6, pp. 1596–1606, Jun. 1982, doi: 10.1109/TPAS.1982.317209.

[11] K. Jia, Q. Zhao, T. Feng, and T. Bi, "Distance protection scheme for DC distribution systems based on the high-frequency characteristics of faults," *IEEE Trans. Power Del.*, vol. 35, no. 1, pp. 234–243, Feb. 2020, doi: 10.1109/TPWRD.2019.2909130.

[12] Y. N. Velaga, K. Prabakar, A. Singh, and P. K. Sen, "High-frequency signature-based fault detection for future MV distribution grids," in *Proc. IEEE/IAS 56th Ind. Commercial Power Syst. Tech. Conf. (ICPS)*, Jun. 2020, pp. 1–8, doi: 10.1109/ICPS48389.2020.9176747.

[13] P. Jafarian and M. Sanaye-Pasand, "High-frequency transients-based protection of multiterminal transmission lines using the SVM technique," *IEEE Trans. Power Del.*, vol. 28, no. 1, pp. 188–196, Jan. 2013, doi: 10.1109/TPWRD.2012.2215925.

[14] D. P. S. Gomes, C. Ozansoy, and A. Ulhaq, "High-sensitivity vegetation high-impedance fault detection based on signal's high-frequency contents," *IEEE Trans. Power Del.*, vol. 33, no. 3, pp. 1398–1407, Jun. 2018, doi: 10.1109/TPWRD.2018.2791986.

[15] D. P. S. Gomes, C. Ozansoy, and A. Ulhaq, "Vegetation high-impedance faults' high-frequency signatures via sparse coding," *IEEE Trans. Instrum. Meas.*, vol. 69, no. 7, pp. 5233–5242, Jul. 2020, doi: 10.1109/TIM.2019.2950822.

[16] T. Marxsen. (2015). Vegetation conduction ignition test report—Final. Marxsen Consulting. Accessed: Nov. 2016. [Online]. Available: https://discover.data.vic.gov.au/dataset/powerline-bushfire-safety-program-vegetation-conduction-ignition-test-report

[17] C. Ozansoy and D. P. S. Gomes, "Electrical and physical characterization of Earth faults for diverse bush species," *Eng. Sci. Technol., Int. J.*, vol. 23, no. 5, pp. 1109–1117, Oct. 2020, doi: 10.1016/j.jestch.2020.03.002.

[18] Y. Seferi, A. Arshad, M. H. Syed, G. Burt, and B. G. Stewart, "Effect of sampling rate and sensor bandwidth on measured transient signals in LV AC and DC power systems," in *Proc. IEEE 12th Int. Workshop Appl. Meas. Power Syst. (AMPS)*, Sep. 2022, pp. 1–5, doi: 10.1109/AMPS55790.2022.9978743.

[19] GE Digital Energy. *F60 Feeder Protection System: Instruction Manual*. Accessed: Apr. 5, 2023. [Online]. Available: https://na.eventscloud.com/file_uploads/051c6b2d1eaff0b7ce9e9d780fcb198a_GEF60.pdf

[20] D. Hou, "Detection of high-impedance faults in power distribution systems," in *Proc. Power Syst. Conf., Adv. Metering, Protection, Control, Commun., Distrib. Resour.*, Mar. 2007, pp. 85–95.

CAGIL RAMADAN OZANSOY (Member, IEEE) received the B.Eng. and Ph.D. degrees in electrical/electronic engineering from Victoria University (VU), Melbourne, Australia, in 2002 and 2006, respectively. He is currently an Associate Professor with VU. He teaches electrical engineering with a focus on power and energy systems. His research interests include investigations on how information exchange and communications could play a major role in shaping up the electrical grid of the future: the smart grids, design and development of communication assisted power systems protection, automation, and control applications. He is well known internationally for his investigations in the novel use of the international substation communication standard IEC 61850. More recently, he has been leading research and development projects in novel methods to cut bushfire risk from power lines. He is using machine learning, signal processing, and power line communications concepts in fault monitoring to reduce fire ignition probability of high impedance faults in electrical power networks.

ALADIN ZAYEGH (Life Member, IEEE) received the B.E. degree in electrical engineering from Aleppo University, Aleppo, Syria, and the M.S. and Ph.D. degrees from Claude Bernard University, Lyon, France. He has been with Victoria University (VU), Melbourne, since 1984, and the former Head of the Electrical and Electronic Department, Faculty of Health, Engineering and Science, and the Head of Electrical and Electronic Engineering Postgraduate Research. He is currently an Adjunct Professor with the College of Engineering and Science supervising postgraduate research Ph.D. and Master of Engineering students, participating in the courses accreditation and courses development. He has wide experience in educational institutions and industry. He has been the Deputy Leader of the Smart Energy Research Group, VU, and through his research leadership; he has been a member of the team who has delivered successful research and development projects that led to industry uptake of project outcomes. In 2000, he was a part of the team which received over $3M from the State Government of Victoria to develop the "Chipskill Program" with VU for training and research in the design and development of microelectronics solutions in power systems and biomedical field. He has conducted research, published over 350 publications on his area of expertise and written several book chapters.